INSTITUTE OF PHYSICS PUBLISHING MODELLING AND SIMULATION IN MATERIALS SCIENCE AND ENGINEERING

Modelling Simul. Mater. Sci. Eng. **11** (2003) 251–264 PII: S0965-0393(03)57878-0

Simulations on the growth of dislocation density during Stage 0 deformation in BCC metals

Athanasios Arsenlis[1] **and Meijie Tang**

University of California, Lawrence Livermore National Laboratory, Livermore, CA 94551, USA

E-mail: arsenlis@llnl.gov

Received 16 September 2002, in final form 2 December 2002
Published 3 February 2003
Online at stacks.iop.org/MSMSE/11/251

Abstract

This study focuses on modelling the behaviour of single crystal tantalum in Stage 0 characterized by the large activity of edge dislocations and relative inactivity of screw dislocations. The multiplication of dislocation density is investigated using dislocation dynamics (DD) simulations and a dislocation density based continuum model of single crystal plasticity. The DD simulations are used to guide the constitutive development of the continuum model and to determine its material specific parameters. While not all of the material constants needed by the continuum model can be determined, due to the limited strain histories considered in the simulations, interpreting the DD simulations through a dislocation mechanics based continuum plasticity model allows for the efficient extraction of scaling laws controlling the growth of dislocation density.

1. Introduction

The Stage 0 deformation behaviour of BCC single crystals is considered using two different numerical simulation techniques. A dislocation dynamics (DD) technique and a continuum crystal plasticity technique are used to quantitatively understand the dislocation density multiplication mechanisms operating during the initial stages of plastic deformation in tantalum single crystals. The Stage 0 deformation regime characterizes the initial onset of plastic deformation in well-annealed BCC crystals after the stress–strain curve begins to deviate from the linear elastic behaviour but before the macroscopic yield point and the onset of easy glide typified by the Stage 1 deformation regime. During Stage 0, the dislocation density increases by an order of magnitude from its initial state, and the density is observed to be composed of predominantly long straight screw dislocations.

The quantitative aspects of DD simulations have mostly focused on the interpretation of stress–strain curves and scalar relationships between stress and dislocation density.

[1] Author to whom correspondence should be addressed.

0965-0393/03/020251+14$30.00

DD simulations contain a wealth of information concerning the evolving dislocation structure, which has been described qualitatively through dislocation configuration snapshots at different points during the course of a simulation, that may be more quantitatively described by dislocation density evolution histograms differentiated by Burgers vector and tangent line directions. Quantitative descriptions of the detailed dislocation density evolution have been limited, mostly due to the inability of continuum crystal plasticity theories to interpret the evolution of the complex system. Interpretation of fine scale simulation (DD) results by coarser simulation (continuum visco-plasticity) methods is a crucial component of establishing a multi-scale materials modelling framework.

The most common continuum crystal plasticity models focus on developing a hardening matrix, $H^{\alpha\beta}$, relating the effect of plastic slip on a slip system, β, to an increase in plastic resistance on the other slip systems, α [1–3]. The plastic behaviour of these models is controlled through the evolution of the hardening matrix during the course of plastic deformation. Unfortunately, the results of DD simulations cannot be easily related to the material constants found in these hardening matrices, primarily because the hardening matrices are phenomenological generalizations developed to close a set of equations commonly used in continuum plasticity at macroscopic length scales, and not directly based on any dislocation mechanisms.

Dislocation density based plasticity models [4, 5] are better suited to interpret and incorporate the wealth of information in DD simulations than the slip-system strength based models (employing hardening matrices) due to their richer description of the material state and closer connection to the underlying physical processes—yet, no significant progress has been made to date to establish formal connections with DD simulations. In principle, accurate DD simulations could provide most, if not all, of the data required to determine the material parameters in the density-based models. A few large scale DD simulations, both in terms of the orders of magnitude spanned in dislocation density and of the amount of plastic strain accumulated, would have to be conducted to inform a continuum model that could reasonably predict the large deformation characteristics of crystalline materials, but such DD simulations have yet to be performed due to their computational demands. However, much can be gained from the current capabilities of DD techniques in guiding constitutive model development of coarse grained continuum plasticity models.

In this paper, we will develop and use a continuum plasticity model for the growth and interaction of dislocation density to interpret the averaged behaviour of DD simulations of tantalum single crystals in the Stage 0 deformation regime. The benefits of linking a continuum plasticity model with DD simulations are twofold. First, the understanding of the DD behaviour becomes more quantitative through comparisons with continuum level understanding of the total system. Second, the constitutive equations developed for the continuum model are more physically realistic because they are derived from observations at a finer scale. By considering the entire DD cell as a representative volume element of a continuum simulation, the stress–strain response, the flux history of both the edge and screw dislocation densities, and the edge and screw dislocation density evolution are used to determine the constitutive form of the continuum model. A series of simulations is conducted at two different crystallographic orientations. The first orientation is used to construct the form and the material parameters for the continuum model, and the second is used to compare the prediction of the continuum model with the parameters determined from the previous orientation.

2. DD simulation details

A DD code based on a screw-edge representation of a general dislocation line, previously developed to study the plastic deformation of BCC single crystals at low temperatures [6, 7],

Table 1. The material constants input into both the DD and continuum simulations.

Elastic constants	$\mu = 68.5\,\text{GPa}$
	$\nu = 0.350$
Screw mobility parameters	$l_c = 4.295\,\text{nm}$
	$\nu_D = 10^{13}\,\text{s}^{-1}$
	$v_0 = 2.22 \times 10^5\,\text{m s}^{-1}$
	$\Delta F = 1.298 \times 10^{-19}\,\text{J atom}^{-1}$
	$\tau_p = 248\,\text{MPa}$
	$p = 0.748$
	$q = 1.172$
Burgers vector	$\lvert\boldsymbol{b}\rvert = 2.863\,\text{Å}$

is used here to study the Stage 0 deformation behaviour of BCC single crystals. In the DD simulations, dislocation lines are discretized into piece-wise connected screw-edge segments that move under local stress and interact with surrounding dislocations through their stress fields and short-range reactions. The mobility of the dislocation segments is one of the key inputs to the simulations.

The mobility of screw dislocations in BCC tantalum at the strain rate ($3.7 \times 10^{-4}\,\text{s}^{-1}$) and temperature (160 K) of this study is controlled by the thermal activation of kink-pairs on the dislocation line. The functional form for the activation enthalpy developed by Kocks *et al* [8] was fit to empirical data and used to describe the motion of screw dislocations [6]. The resulting constitutive equation for the screw dislocation segment velocity took the form

$$\bar{v}_s^\alpha = \frac{Lb^2}{l_c^2}\nu_D \exp\left[-\frac{\Delta F}{k\theta}\left(1 - \left(\frac{|\tau^\alpha|}{\tau_p}\right)^p\right)^q\right]\text{sign}(\tau^\alpha), \tag{1}$$

with

$$\tau^\alpha = \boldsymbol{m}^\alpha \cdot \bar{\boldsymbol{T}}\boldsymbol{n}^\alpha, \tag{2}$$

where L is the segment length of the mobile screw dislocation, b the magnitude of the burgers vector, l_c the critical length for double kink nucleation, ν_D the Debye frequency, ΔF the activation enthalpy of kink-pair formation, k the Boltzmann constant, θ the absolute temperature, τ_p the Peierls barrier, p and q are exponents detailing the effect of stress on the kink formation enthalpy, $\boldsymbol{m}^\alpha$ is the Burgers vector direction of the gliding segment, $\boldsymbol{n}^\alpha$ the glide plane, and $\bar{\boldsymbol{T}}$ the local value stress tensor at the position of the screw dislocation segment. The values of the material constants may be found in table 1.

The mobility of the edge dislocations in the temperature and strain rate considered is limited by phonon drag, and it is known to be orders of magnitude larger than that of screws. The edges were treated as infinitely fast in the DD simulations allowing for a significant gain in computation efficiency. The edge dislocations arrested only in positions of local equilibrium or in positions where they formed junctions with other dislocations. To model strain hardening, dislocation junctions were simulated with an average junction strength parameter obtained from experimental data [7].

Due to the large difference between the screw and edge mobilities, there exists a characteristic Stage 0 plastic deformation for BCC single crystals defined as the early stage of deformation before the macro-yield point is reached [9]. During Stage 0, the plastic flow is carried out mainly by fast moving edge dislocations. The microstructural evolution is characterized by a large density increase of extended screw dislocations on multiple slip systems due to the motion of those highly mobile edge dislocations [10]. We have simulated the Stage 0 plastic deformation of single crystal tantalum for two families of single slip orientations, i.e. ⟨4 8 19⟩ and ⟨1 2 3⟩.

Table 2. Catalogue of slip systems used in both the DD and dislocation density based continuum simulations.

Slip system index	$\boldsymbol{m}$	$\boldsymbol{n}$
1	[111]	$(01\bar{1})$
2	[111]	$(\bar{1}01)$
3	[111]	$(1\bar{1}0)$
4	$[\bar{1}11]$	$(\bar{1}0\bar{1})$
5	$[\bar{1}11]$	$(0\bar{1}1)$
6	$[\bar{1}11]$	(110)
7	$[\bar{1}\bar{1}1]$	$(0\bar{1}\bar{1})$
8	$[\bar{1}\bar{1}1]$	(101)
9	$[\bar{1}\bar{1}1]$	$(\bar{1}10)$
10	$[1\bar{1}1]$	$(10\bar{1})$
11	$[1\bar{1}1]$	(011)
12	$[1\bar{1}1]$	$(\bar{1}\bar{1}0)$

The simulations were performed under conditions of uniaxial tension at 160 K and at a constant tensile strain rate of $3.7 \times 10^{-4}\,\mathrm{s}^{-1}$. The dislocation density was constrained to lie in the twelve $\langle 1\ 1\ 1\rangle$ $\{1\ 1\ 0\}$ slip systems indexed in table 2, and the initial dislocation configuration contained a total density of $10^{11}\,\mathrm{m}^{-2}$ composed of screw and edge dislocations uniformly distributed over all the slip systems. The initial dislocation segment lengths were randomly distributed around an average value of 1 μm. Isotropic elastic constants [11], given in table 1, were used to approximate the anistropic elastic constants of tantalum at 160 K for computational efficiency in the DD simulations.

The simulations were terminated at the end of Stage 0, which we defined as the point when the plastic strain rate reached the applied strain rate. While keeping the initial dislocation configuration constant, the tensile stress was applied to each of the twenty-four equivalent directions within each orientation family. The typical simulation box was orthorhombic with lateral dimensions ranging from 15 to 18 μm, and periodic boundary conditions were imposed to simulate the behaviour of a bulk crystal. The dimensions of the simulation boxes were deliberately chosen to avoid unnatural dislocation self-annihilation due to the imposed periodic boundary conditions [12].

The tensile stress, density evolution history, and flux history of the edge and screw dislocations on all the slip systems were output by the series of simulations. The data from each orientation family was averaged to reduce the noise associated with a single DD simulation. Figure 1 depicts a typical dislocation configuration at the end of Stage 0 as calculated by the DD method, and figure 2 depicts the raw data that was extracted and used to develop and test a continuum level understanding of the discrete system.

3. Continuum model description

The single crystal continuum model developed to interpret the results of the DD simulations can be categorized as an internal state variable model in which crystallographic dislocation densities, their average segment lengths, and the elastic deformation gradient completely describe the state of the crystal. It is an extension of a crystal plasticity model developed previously by Arsenlis and Parks [5]. The dislocation densities are crystallographic in the sense that two dislocation densities for each crystal slip system are used to capture the general dislocation state of the crystal similar to the manner in which general dislocation lines are

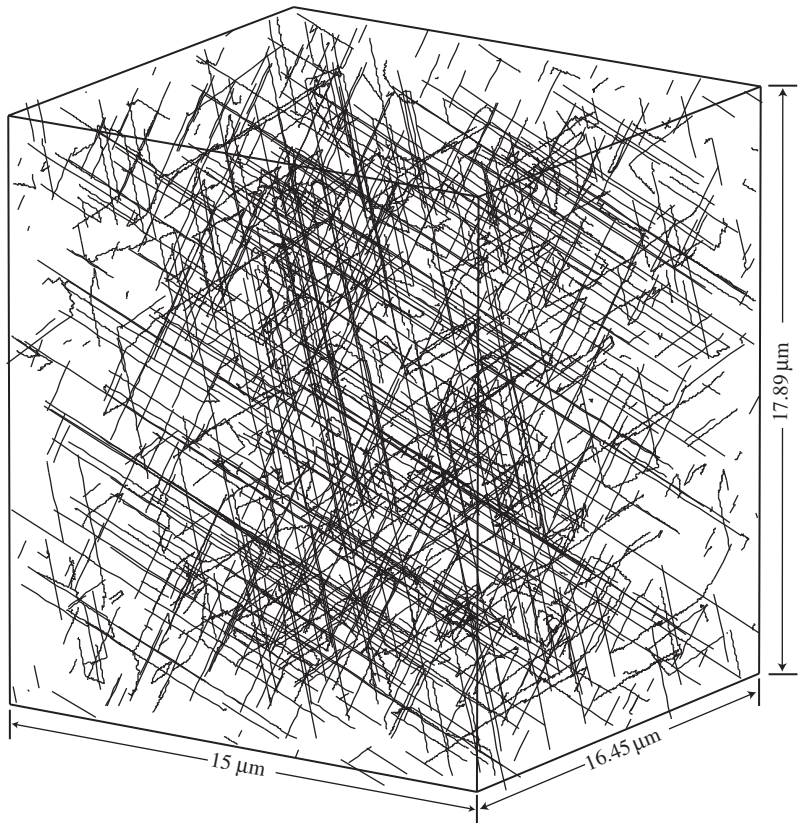

Figure 1. Dislocation configuration, with a total density of $1.2 \times 10^{12}\ \mathrm{m}^{-2}$, at the end of Stage 0 for a crystal oriented with the [8 $\bar{4}$ 19] direction parallel to the tensile axis. The orthorhombic shape of the simulation box limits the spurious annihilation of density due to periodic boundary conditions.

decomposed into piece-wise connected screw-edge segments in the DD simulations. Since the screw and edge (non-screw) dislocations behave differently in BCC crystals, a state variable is assigned to capture the density of each on every slip system. The dislocation density evolution equations will focus on the statistical generation of density solely and not the statistical annihilation of density due to the small strains considered.

Although the study is presently limited to small strains, the continuum model will be developed with the intent to extrapolate the plastic behaviour at large strains based on the DD results at small strains. The large deformation kinematics of Asaro and Rice [13] are employed in which the total deformation gradient, $\boldsymbol{F}$, is multiplicatively decomposed into an elastic, $\boldsymbol{F}^{\mathrm{e}}$, and plastic, $\boldsymbol{F}^{\mathrm{p}}$, component such that

$$\boldsymbol{F} = \boldsymbol{F}^{\mathrm{e}}\boldsymbol{F}^{\mathrm{p}}. \tag{3}$$

A stress measure, $\bar{\boldsymbol{T}}$, corresponding to the second Piola–Kirchhoff stress in the intermediate configuration is defined as

$$\bar{\boldsymbol{T}} = \det(\boldsymbol{F}^{\mathrm{e}})\boldsymbol{F}^{\mathrm{e}-1}\boldsymbol{T}\boldsymbol{F}^{\mathrm{e}-\mathrm{T}}, \tag{4}$$

where $\boldsymbol{T}$ is the Cauchy stress. The stress measure, $\bar{\boldsymbol{T}}$, is related to an elastic strain measure, $\boldsymbol{E}^{\mathrm{e}} = \frac{1}{2}\{\boldsymbol{F}^{\mathrm{e}\mathrm{T}}\boldsymbol{F}^{\mathrm{e}} - \boldsymbol{I}_2\}$, corresponding to Cauchy–Green strain in the intermediate configuration,

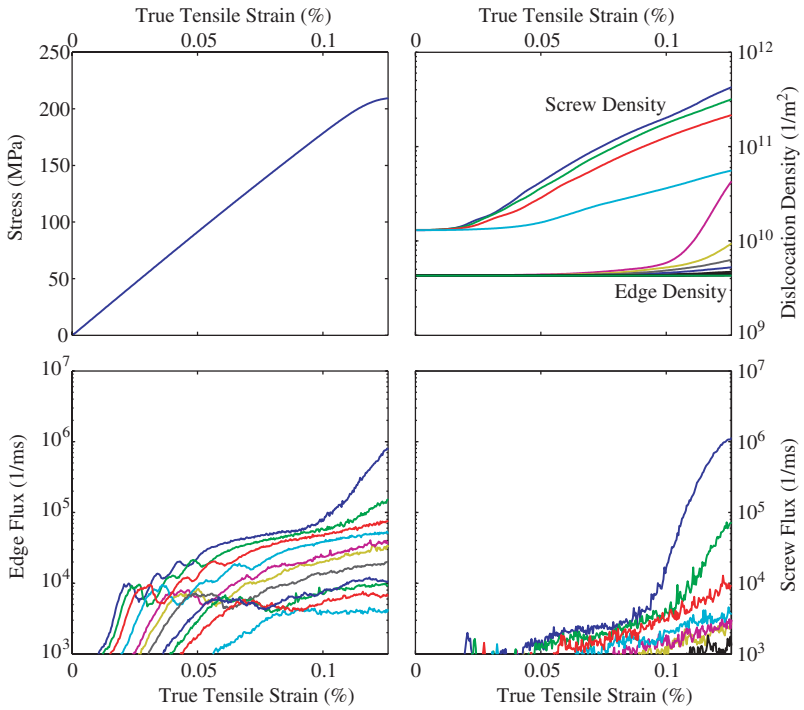

Figure 2. Data output from the DD simulations in the ⟨4 8 19⟩ family of orientations used as input for fitting the material parameters of the continuum model. The data is averaged over 24 orientations, and the behaviour of all twelve slip systems is followed.

by the fourth order elasticity tensor $\mathcal{L}$, through the expression

$$\bar{\boldsymbol{T}} \equiv \mathcal{L}[\boldsymbol{E}^{\mathrm{e}}]. \tag{5}$$

The plastic deformation gradient evolves according to the flow rule

$$\dot{\boldsymbol{F}}^{\mathrm{p}} = \boldsymbol{L}^{\mathrm{p}}\boldsymbol{F}^{\mathrm{p}}, \tag{6}$$

where $\boldsymbol{L}^{\mathrm{p}}$ is the plastic flow rate composed of the tensorial sum of the crystallographic plastic shear rates, $\dot{\gamma}^{\alpha}$, such that

$$\boldsymbol{L}^{\mathrm{p}} = \sum_{\alpha} \dot{\gamma}^{\alpha} \boldsymbol{m}^{\alpha} \otimes \boldsymbol{n}^{\alpha} \ , \tag{7}$$

where $\boldsymbol{m}^{\alpha}$ and $\boldsymbol{n}^{\alpha}$ are unit lattice vectors in the intermediate configuration corresponding to the slip direction and the slip plane normal direction, respectively, for a given slip system α. The crystallographic plastic shear rates result from the combined motion of edge and screw dislocation densities, $\rho_{\mathrm{e}}^{\alpha}$ and $\rho_{\mathrm{s}}^{\alpha}$. Following Orowan's relation,

$$\dot{\gamma}^{\alpha} = \rho_{\mathrm{e}}^{\alpha} b \bar{v}_{\mathrm{e}}^{\alpha} + \rho_{\mathrm{s}}^{\alpha} b \bar{v}_{\mathrm{s}}^{\alpha}, \tag{8}$$

where b is the magnitude of the Burgers vector, and $\bar{v}_{\mathrm{e}}^{\alpha}$ and $\bar{v}_{\mathrm{s}}^{\alpha}$ are the average velocities of the edge and screw dislocation densities, respectively.

The dislocation densities evolve with plastic deformation according to

$$\dot{\rho}_{\mathrm{e}}^{\alpha} = \frac{2\rho_{\mathrm{s}}^{\alpha}|\bar{v}_{\mathrm{s}}^{\alpha}|}{\bar{l}_{\mathrm{s}}^{\alpha}}, \tag{9}$$

$$\dot{\rho}_{\mathrm{s}}^{\alpha} = \frac{2\rho_{\mathrm{e}}^{\alpha}|\bar{v}_{\mathrm{e}}^{\alpha}|}{\bar{l}_{\mathrm{e}}^{\alpha}}, \tag{10}$$

where $\bar{l}_{\mathrm{e}}^{\alpha}$ and $\bar{l}_{\mathrm{s}}^{\alpha}$ are the average segment lengths for the edge and screw densities, respectively [5]. Equations (9) and (10) capture the dislocation density generated by mobile dislocation segments leaving dislocation dipoles in their wake. Snapshots of the dislocation configuration in the DD simulations clearly show this mechanism of dislocation growth due to the disparity in the mobility between the edge and screw segments.

The average segment lengths evolve with plastic deformation according to

$$\dot{\bar{l}}_{\mathrm{e}}^{\alpha} = \frac{\bar{l}_{\mathrm{e}}^{\alpha}}{\rho_{\mathrm{e}}^{\alpha}}\dot{\rho}_{\mathrm{e}}^{\alpha} - \left(\bar{l}_{\mathrm{e}}^{\alpha}\right)^{3}\left(H_{\mathrm{ee}}^{\alpha\beta}\dot{\rho}_{\mathrm{e}}^{\beta} + H_{\mathrm{es}}^{\alpha\beta}\dot{\rho}_{\mathrm{s}}^{\beta}\right), \tag{11}$$

$$\dot{\bar{l}}_{\mathrm{s}}^{\alpha} = \frac{\bar{l}_{\mathrm{s}}^{\alpha}}{\rho_{\mathrm{s}}^{\alpha}}\dot{\rho}_{\mathrm{s}}^{\alpha} - \left(\bar{l}_{\mathrm{s}}^{\alpha}\right)^{3}\left(H_{\mathrm{se}}^{\alpha\beta}\dot{\rho}_{\mathrm{e}}^{\beta} + H_{\mathrm{ss}}^{\alpha\beta}\dot{\rho}_{\mathrm{s}}^{\beta}\right), \tag{12}$$

where $H_{\mathrm{ee}}^{\alpha\beta}$, $H_{\mathrm{es}}^{\alpha\beta}$, $H_{\mathrm{se}}^{\alpha\beta}$ and $H_{\mathrm{ss}}^{\alpha\beta}$ are the average segment length interaction matrices [5]. The first terms in equations (11) and (12) capture the elongation of dislocation line segments as density is generated by the dipole mechanism outlined above, and the second term in each of the equations captures the shortening of the average dislocation length as dislocation sources inject nascent loops into the crystal. The dislocation density and average segment length combine to quantify the total dislocation line length and number density of dislocations per unit volume.

To close the model, constitutive equations are required for the average segment length interaction matrices, and the average dislocation velocities. The average segment length interaction matrices will be assumed constant, with the value of the constants to be determined from the DD simulations. The average dislocation velocity functions for the edge and screw dislocation densities will take different forms due to the kink-pair formation mechanism controlling screw dislocation motion and the high mobility of edge (non-screw) dislocation density. The average velocity function for the screw density will be the same as the velocity function in the DD simulation for the screw dislocation segments found in equation (1). Whereas the glide activity of each individual screw dislocation was a function of each segment's length, the length of the screw dislocation density associated with equation (1) was assumed to be constant during the continuum simulation. The stress dependence of the screw velocity is more sensitive to the material parameters inside the exponential and not as sensitive to the pre-exponential terms so long as the correct order of magnitude is input for those terms. A representative value of 5 μm was used for L in equation (1) in the continuum simulations.

The glide activity of the screw dislocation density is limited to the end of the DD simulations, and their motion is dominated by their ability to nucleate a kink-pair and not by forest type interactions with other dislocations. Therefore, any interaction with the forest density that affects the motion of the screw density will be neglected in the continuum model. Various constitutive forms for the interaction between dislocations in BCC crystals have been previously suggested [7, 14]; however, there is not enough information in the histograms depicted in figure 2 to determine the appropriate function.

The infinite mobility of the edge dislocations in the DD simulations is impossible to implement in a continuum model because the discrete dislocation positions are not defined in the continuum simulation; therefore, an empirical power law dependence [15] will be employed for the edge velocity, of the form

$$\bar{v}_{\mathrm{e}}^{\alpha} = B\left(\tau^{\alpha} - \mu b\sqrt{G_{\mathrm{ee}}^{\alpha\beta}\rho_{\mathrm{e}}^{\beta} + G_{\mathrm{es}}^{\alpha\beta}\rho_{\mathrm{s}}^{\beta}}\right)^{n}, \tag{13}$$

where B is a reference edge mobility factor, n the stress sensitivity, and $G_{\mathrm{ee}}^{\alpha\beta}$ and $G_{\mathrm{es}}^{\alpha\beta}$ are the dislocation strength interaction matrices for gliding edge dislocation density. A square root dependence on the dislocation density was chosen for the forest resistance. Although the

infinite edge mobility acted to speed up the DD simulations, it hindered the extraction of the correct scaling law of the dislocation resistance; therefore, the simple square root dependence commonly used in FCC crystals was assumed [16].

4. Continuum model parameter estimation

The results of the ⟨4 8 19⟩ tensile tests, depicted in figure 2, and the material constants input to the DD simulations [6] were used to determine the material constants in the continuum constitutive equations. The elastic constants, magnitude of the Burgers vector, and screw mobility parameters found in table 1 were taken directly from the input values of the DD simulations. The values of the edge mobility parameters and of the average segment length matrix coefficients had to be determined by fitting the continuum constitutive functions to the aggregate dislocation segment behaviour of the DD simulations.

The representation of general dislocation lines by piece-wise connected edge and screw segments allowed for a simple extraction of the average velocity of the edge densities. The crystallographic fluxes, defined as the product of the crystallographic densities and their respective velocities, were simply divided by the dislocation density associated with that flux to extract the average velocities of all twelve edge dislocation densities in the crystal. Taking the symmetry of the BCC crystal into account, there are seven unique coefficients in the $G_{\mathrm{ee}}^{\alpha\beta}$ matrix and three unique coefficients in the $G_{\mathrm{es}}^{\alpha\beta}$ matrix. The positions of the coefficients in the matrices are given in table 3, and the matrix indices correspond to the list of slip systems given

Table 3. Strength interaction matrices, $G_{\mathrm{ee}}^{\alpha\beta}$ and $G_{\mathrm{es}}^{\alpha\beta}$, between the gliding edge density and the forest edge and screw densities, respectively. The average segment length interaction matrices, $H_{\mathrm{ee}}^{\alpha\beta}$, $H_{\mathrm{es}}^{\alpha\beta}$, $H_{\mathrm{se}}^{\alpha\beta}$ and $H_{\mathrm{ss}}^{\alpha\beta}$; take the same form, but with different values. The coefficient values determined by fitting the constitutive functions to the DD results are given below.

$$\left[G_{\mathrm{ee}}^{\alpha\beta}\right]_{\substack{\alpha=1,12\\ \beta=1,12}} = \begin{bmatrix}
G_{\mathrm{ee}}^{0} & G_{\mathrm{ee}}^{2} & G_{\mathrm{ee}}^{2} & G_{\mathrm{ee}}^{3} & G_{\mathrm{ee}}^{1} & G_{\mathrm{ee}}^{3} & G_{\mathrm{ee}}^{5} & G_{\mathrm{ee}}^{6} & G_{\mathrm{ee}}^{4} & G_{\mathrm{ee}}^{4} & G_{\mathrm{ee}}^{5} & G_{\mathrm{ee}}^{6} \\
G_{\mathrm{ee}}^{2} & G_{\mathrm{ee}}^{0} & G_{\mathrm{ee}}^{2} & G_{\mathrm{ee}}^{5} & G_{\mathrm{ee}}^{4} & G_{\mathrm{ee}}^{6} & G_{\mathrm{ee}}^{6} & G_{\mathrm{ee}}^{5} & G_{\mathrm{ee}}^{4} & G_{\mathrm{ee}}^{1} & G_{\mathrm{ee}}^{3} & G_{\mathrm{ee}}^{3} \\
G_{\mathrm{ee}}^{2} & G_{\mathrm{ee}}^{2} & G_{\mathrm{ee}}^{0} & G_{\mathrm{ee}}^{6} & G_{\mathrm{ee}}^{4} & G_{\mathrm{ee}}^{5} & G_{\mathrm{ee}}^{3} & G_{\mathrm{ee}}^{3} & G_{\mathrm{ee}}^{1} & G_{\mathrm{ee}}^{4} & G_{\mathrm{ee}}^{6} & G_{\mathrm{ee}}^{5} \\
G_{\mathrm{ee}}^{4} & G_{\mathrm{ee}}^{5} & G_{\mathrm{ee}}^{6} & G_{\mathrm{ee}}^{0} & G_{\mathrm{ee}}^{2} & G_{\mathrm{ee}}^{2} & G_{\mathrm{ee}}^{3} & G_{\mathrm{ee}}^{1} & G_{\mathrm{ee}}^{3} & G_{\mathrm{ee}}^{5} & G_{\mathrm{ee}}^{6} & G_{\mathrm{ee}}^{4} \\
G_{\mathrm{ee}}^{1} & G_{\mathrm{ee}}^{3} & G_{\mathrm{ee}}^{3} & G_{\mathrm{ee}}^{2} & G_{\mathrm{ee}}^{0} & G_{\mathrm{ee}}^{2} & G_{\mathrm{ee}}^{5} & G_{\mathrm{ee}}^{4} & G_{\mathrm{ee}}^{6} & G_{\mathrm{ee}}^{6} & G_{\mathrm{ee}}^{5} & G_{\mathrm{ee}}^{4} \\
G_{\mathrm{ee}}^{4} & G_{\mathrm{ee}}^{6} & G_{\mathrm{ee}}^{5} & G_{\mathrm{ee}}^{2} & G_{\mathrm{ee}}^{2} & G_{\mathrm{ee}}^{0} & G_{\mathrm{ee}}^{6} & G_{\mathrm{ee}}^{4} & G_{\mathrm{ee}}^{5} & G_{\mathrm{ee}}^{3} & G_{\mathrm{ee}}^{3} & G_{\mathrm{ee}}^{1} \\
G_{\mathrm{ee}}^{5} & G_{\mathrm{ee}}^{6} & G_{\mathrm{ee}}^{4} & G_{\mathrm{ee}}^{4} & G_{\mathrm{ee}}^{5} & G_{\mathrm{ee}}^{6} & G_{\mathrm{ee}}^{0} & G_{\mathrm{ee}}^{2} & G_{\mathrm{ee}}^{2} & G_{\mathrm{ee}}^{3} & G_{\mathrm{ee}}^{1} & G_{\mathrm{ee}}^{3} \\
G_{\mathrm{ee}}^{6} & G_{\mathrm{ee}}^{5} & G_{\mathrm{ee}}^{4} & G_{\mathrm{ee}}^{1} & G_{\mathrm{ee}}^{3} & G_{\mathrm{ee}}^{3} & G_{\mathrm{ee}}^{2} & G_{\mathrm{ee}}^{0} & G_{\mathrm{ee}}^{2} & G_{\mathrm{ee}}^{5} & G_{\mathrm{ee}}^{4} & G_{\mathrm{ee}}^{6} \\
G_{\mathrm{ee}}^{3} & G_{\mathrm{ee}}^{3} & G_{\mathrm{ee}}^{1} & G_{\mathrm{ee}}^{4} & G_{\mathrm{ee}}^{6} & G_{\mathrm{ee}}^{5} & G_{\mathrm{ee}}^{2} & G_{\mathrm{ee}}^{2} & G_{\mathrm{ee}}^{0} & G_{\mathrm{ee}}^{6} & G_{\mathrm{ee}}^{4} & G_{\mathrm{ee}}^{5} \\
G_{\mathrm{ee}}^{3} & G_{\mathrm{ee}}^{1} & G_{\mathrm{ee}}^{3} & G_{\mathrm{ee}}^{5} & G_{\mathrm{ee}}^{6} & G_{\mathrm{ee}}^{4} & G_{\mathrm{ee}}^{4} & G_{\mathrm{ee}}^{5} & G_{\mathrm{ee}}^{6} & G_{\mathrm{ee}}^{0} & G_{\mathrm{ee}}^{2} & G_{\mathrm{ee}}^{2} \\
G_{\mathrm{ee}}^{5} & G_{\mathrm{ee}}^{4} & G_{\mathrm{ee}}^{6} & G_{\mathrm{ee}}^{6} & G_{\mathrm{ee}}^{5} & G_{\mathrm{ee}}^{1} & G_{\mathrm{ee}}^{1} & G_{\mathrm{ee}}^{3} & G_{\mathrm{ee}}^{3} & G_{\mathrm{ee}}^{2} & G_{\mathrm{ee}}^{0} & G_{\mathrm{ee}}^{2} \\
G_{\mathrm{ee}}^{6} & G_{\mathrm{ee}}^{4} & G_{\mathrm{ee}}^{5} & G_{\mathrm{ee}}^{3} & G_{\mathrm{ee}}^{3} & G_{\mathrm{ee}}^{4} & G_{\mathrm{ee}}^{4} & G_{\mathrm{ee}}^{6} & G_{\mathrm{ee}}^{5} & G_{\mathrm{ee}}^{2} & G_{\mathrm{ee}}^{2} & G_{\mathrm{ee}}^{0}
\end{bmatrix}$$

$$\left[G_{\mathrm{es}}^{\alpha\beta}\right] = \begin{bmatrix}
G_{\mathrm{es}}^{0} & G_{\mathrm{es}}^{1} & G_{\mathrm{es}}^{6} & G_{\mathrm{es}}^{6} \\
G_{\mathrm{es}}^{0} & G_{\mathrm{es}}^{6} & G_{\mathrm{es}}^{6} & G_{\mathrm{es}}^{1} \\
G_{\mathrm{es}}^{0} & G_{\mathrm{es}}^{6} & G_{\mathrm{es}}^{1} & G_{\mathrm{es}}^{6} \\
G_{\mathrm{es}}^{6} & G_{\mathrm{es}}^{0} & G_{\mathrm{es}}^{1} & G_{\mathrm{es}}^{6} \\
G_{\mathrm{es}}^{1} & G_{\mathrm{es}}^{0} & G_{\mathrm{es}}^{6} & G_{\mathrm{es}}^{6} \\
G_{\mathrm{es}}^{6} & G_{\mathrm{es}}^{0} & G_{\mathrm{es}}^{6} & G_{\mathrm{es}}^{1} \\
G_{\mathrm{es}}^{6} & G_{\mathrm{es}}^{6} & G_{\mathrm{es}}^{0} & G_{\mathrm{es}}^{1} \\
G_{\mathrm{es}}^{6} & G_{\mathrm{es}}^{1} & G_{\mathrm{es}}^{0} & G_{\mathrm{es}}^{6} \\
G_{\mathrm{es}}^{1} & G_{\mathrm{es}}^{6} & G_{\mathrm{es}}^{0} & G_{\mathrm{es}}^{6} \\
G_{\mathrm{es}}^{1} & G_{\mathrm{es}}^{6} & G_{\mathrm{es}}^{6} & G_{\mathrm{es}}^{0} \\
G_{\mathrm{es}}^{6} & G_{\mathrm{es}}^{6} & G_{\mathrm{es}}^{1} & G_{\mathrm{es}}^{0} \\
G_{\mathrm{es}}^{6} & G_{\mathrm{es}}^{1} & G_{\mathrm{es}}^{6} & G_{\mathrm{es}}^{0}
\end{bmatrix}$$

Fitted strength interaction coefficients:

$G_{\mathrm{ee}}^{0} = G_{\mathrm{ee}}^{2} = G_{\mathrm{ee}}^{3} = G_{\mathrm{ee}}^{4} = G_{\mathrm{ee}}^{5} = 0,$

$G_{\mathrm{ee}}^{1} = 1,\ G_{\mathrm{ee}}^{6} = 2.89 \times 10^{-1}$

$G_{\mathrm{es}}^{0} = 8.60 \times 10^{-2}, G_{\mathrm{es}}^{1} = 0,$

$G_{\mathrm{es}}^{6} = 3.47 \times 10^{-2}$

Fitted length interaction coefficients:

$H_{\mathrm{ee}}^{0} = H_{\mathrm{ee}}^{1} = H_{\mathrm{ee}}^{2} = H_{\mathrm{ee}}^{3} = 0.00$

$H_{\mathrm{ee}}^{4} = H_{\mathrm{ee}}^{5} = H_{\mathrm{ee}}^{6} = 0.00,$

$H_{\mathrm{es}}^{0} = H_{\mathrm{es}}^{1} = H_{\mathrm{es}}^{6} = 0.00,$

$H_{\mathrm{se}}^{0} = H_{\mathrm{se}}^{1} = H_{\mathrm{se}}^{2} = H_{\mathrm{se}}^{4} = H_{\mathrm{se}}^{5} = 0.00,$

$H_{\mathrm{se}}^{3} = 1.44 \times 10^{2},\ H_{\mathrm{se}}^{6} = 1.12 \times 10^{1},$

$H_{\mathrm{ss}}^{0} = H_{\mathrm{ss}}^{1} = 0,\ H_{\mathrm{ss}}^{6} = 2.01 \times 10^{-2}$

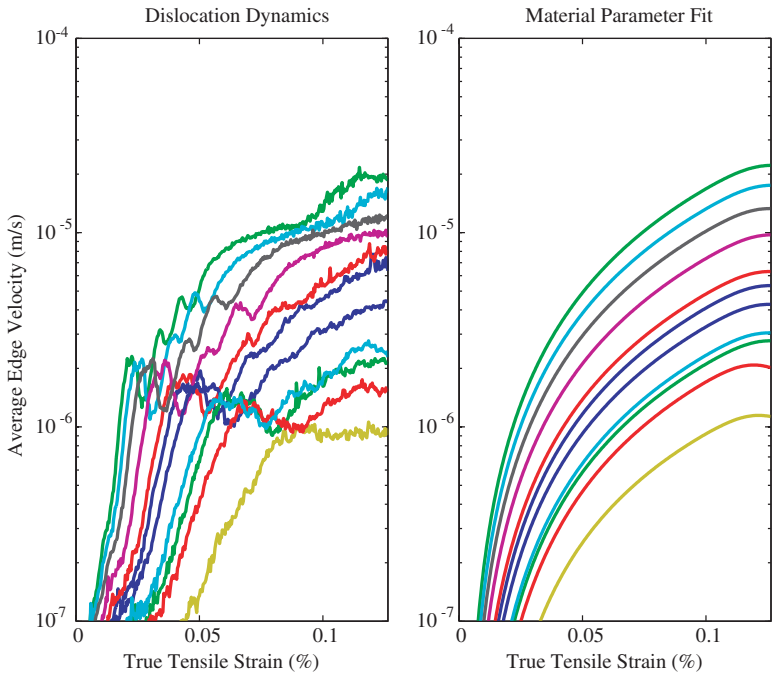

Figure 3. Comparison of the average edge dislocation velocities from the DD simulations of the ⟨4 8 19⟩ orientation family and the continuum constitutive function in equation (13) with fitted material parameters. The eleven curves in each subplot are the edge velocities on the different slip systems in the crystal.

in table 2. The $G_{\text{es}}^{\alpha\beta}$ matrix shown has been compressed by summing the screw dislocation densities with the same Burgers vector before multiplying them by the interaction matrix. Along with the the reference edge mobility factor, B, and stress sensitivity, n, a total of twelve material parameters were simultaneously fit to the output of the DD simulation.

The fit was conducted by minimizing the error between the logarithms of the average velocities in the DD simulation and the velocities from the constitutive function in equation (13) for the eleven edge velocities that rose above the simulation noise level with the constraint that the strength interaction coefficients lie between zero and unity. The quality of the fitting procedure can be seen in figure 3, and the values of the strength interaction coefficients are found in table 3. The best-fit values for B and n were 5.50×10^{-9} m s^{-1} and 1.81, respectively.

After the constitutive equations for the average edge dislocation velocities were fit, the material parameters controlling the dislocation density evolution were determined using the continuum velocity functions and the initial dislocation densities of the DD simulations. Equations (9) and (10) were numerically integrated to generate dislocation density histories for comparison to the dislocation density histories output by the DD simulations. Attempts to fit the dislocation density evolution using constitutive equations for the average segment length previously developed [4,5] failed because the average segment length in those models is proportional to the inverse square root of the dislocation density. As the density increases, the average segment length is assumed to decrease in those constitutive models. Using the inverse square root dependent constitutive functions led to systematic overestimates of the dislocation density near the macro-yield point.

Although the inverse square root scaling may hold at moderate strains, Stage 0 deformation in BCC metals leads to longer screw dislocation segments with increasing density, a property

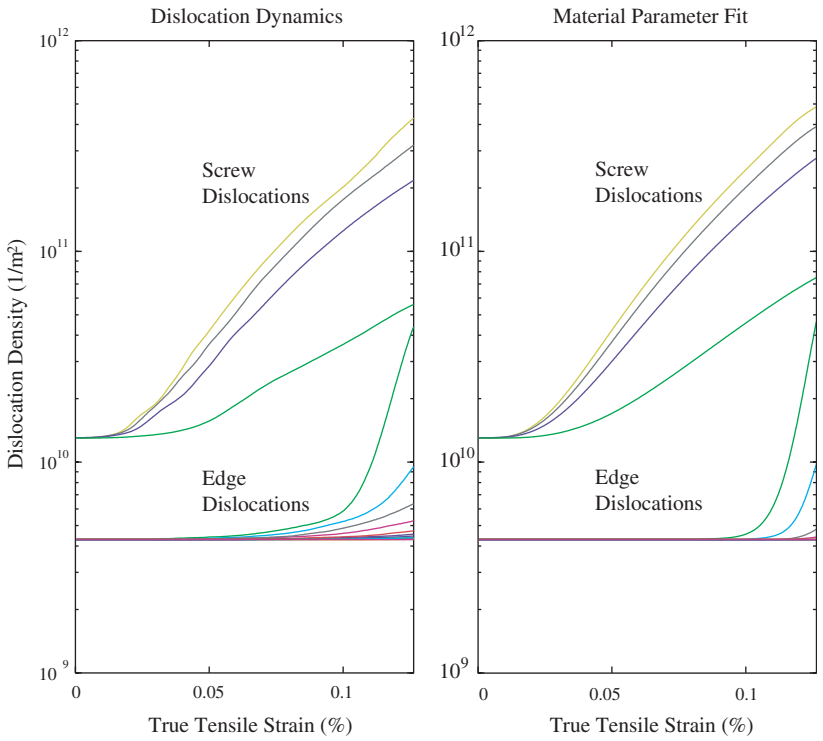

Figure 4. Comparison of the dislocation density evolution from the DD simulations of the ⟨4 8 19⟩ orientation family and the continuum constitutive functions in equations (9)–(12) with fitted material parameters. The screw densities sharing a Burgers vector are consolidated, and all twelve crystallographic edge densities in the crystal are plotted.

of the dislocation density that those constitutive equations fails to capture. The constitutive equations for the average dislocation segment length of Arsenlis and Parks [5] were modified to include the lengthening of dislocation segments with dislocation loop expansion forming the average segment length evolution equations in equations (11) and (12), and the systematic error was eliminated. With the equations proposed, the inverse square root scaling of the average segment length would be retained at larger strains associated with higher density levels. To bolster confidence in our evolution equations, the initial dislocation segment lengths along with the coefficients in the length interaction matrices, were fit to the DD simulation profiles. The symmetry of the length interaction matrices, $H^{\alpha\beta}$, was assumed to be the same as for the strength interaction matrices, $G^{\alpha\beta}$, reducing the number of interaction coefficients that had to be found from 576 to 20. With the constraint that the length interaction coefficients be non-negative, the error between the logarithm of the dislocation density histories from the DD simulations and the integrated continuum evolution equations was minimized to determine the 20 constants and initial dislocation segment length simultaneously. An initial segment length of 1 μm, the same value input to the DD simulations, was found to best fit the dislocation evolution data. The independent confirmation of the initial segment length led us to believe that the underlying physical processes controlling dislocation accumulation were being captured correctly by the continuum model. The results of the fitting procedure for the dislocation evolution are shown graphically in figure 4, and the values of the segment length interaction matrix coefficients are given in table 3.

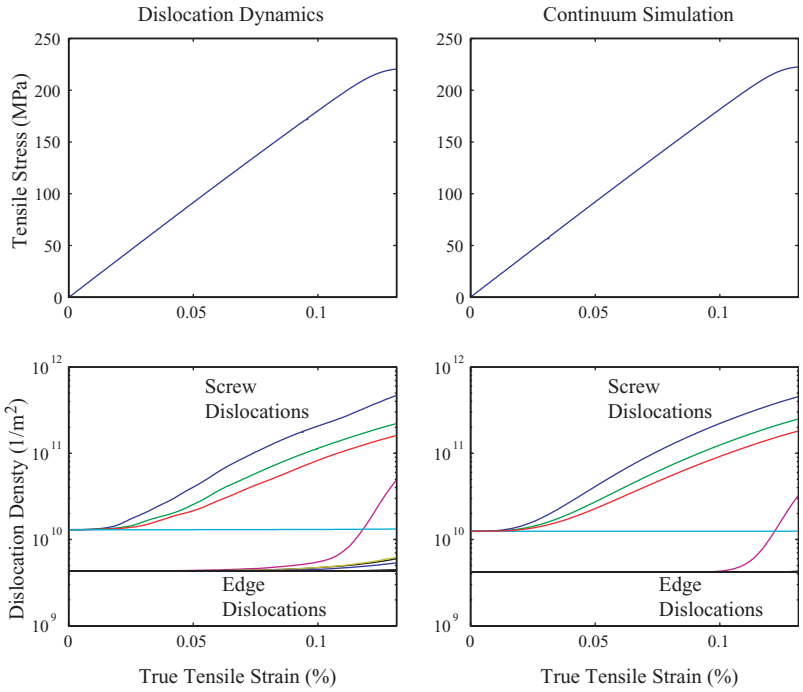

Figure 5. Continuum prediction of the stress–strain behaviour and dislocation density evolution of a ⟨1 2 3⟩ oriented crystal in uniaxial tension compared to the average behaviour of the DD simulations under the same loading conditions. The screw densities sharing a Burgers vector are consolidated, and all twelve crystallographic edge densities in the crystal are plotted.

5. Model comparisons and discussion

Using the constitutive function parameters fit to the simulated behaviour of the ⟨4 8 19⟩ oriented crystal, the continuum model was used to predict the behaviour of a crystal with the [1 2 3] direction parallel to the tensile axis. The purpose of the predictions was to test how well the system of constitutive equations reproduced the growth of dislocation density observed in the DD simulations and to validate our understanding of the scaling laws governing that growth. The predictions of the continuum model are compared to results of the averaged DD simulations in figures 5 and 6. By all measures—stress–strain response, dislocation density evolution, edge density flux, and screw density flux—the continuum model agrees well with the more complex DD simulations for this new orientation. The macro-yield point of the stress–strain response is predicted to within 2%, and although the stress–strain response appears to be purely linear elastic during below 0.1% strain, the edge density flux and the associated screw density evolution, at that strain regime, show evidence of micro-yielding.

The dislocation density evolution is also well predicted. The screw density accumulates with the motion of the edge density during the course of the simulation, and the relative densities of the screw dislocations with different Burgers vectors is well predicted. Furthermore, the mechanism of screw dislocation multiplication is solely due to the motion of the initial edge dislocation segments within the system, which is deduced from the fact that the best-fit coefficients for the $H_{\mathrm{ee}}^{\alpha\beta}$ and $H_{\mathrm{es}}^{\alpha\beta}$ are zero (see table 3). Interpretation of the evolution history of the screw dislocation density with the appropriate physics-based constitutive equations leads

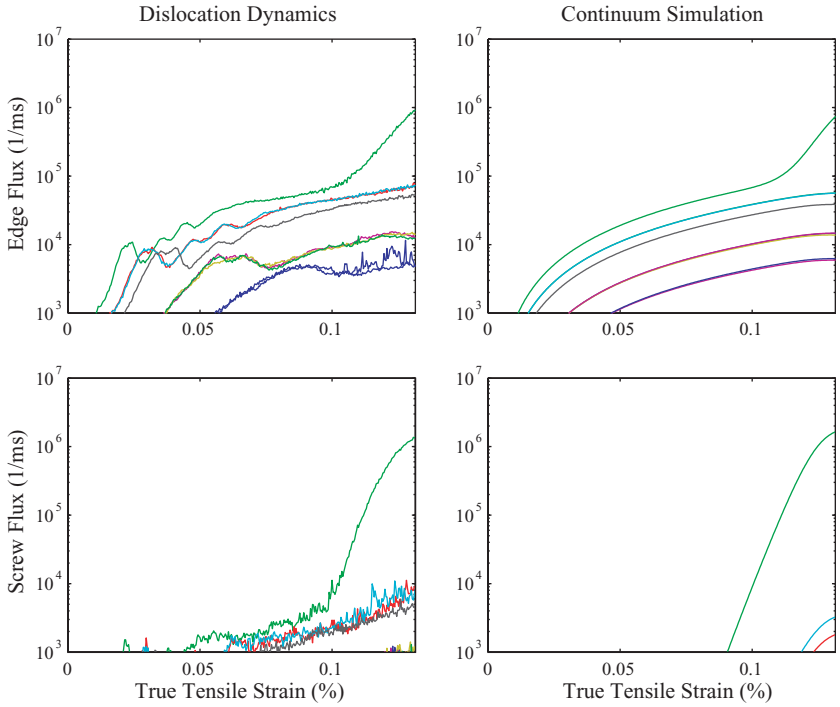

Figure 6. Continuum prediction of the edge and screw dislocation density flux history of a ⟨1 2 3⟩ oriented crystal in uniaxial tension compared to the average behaviour of the DD simulations under the same loading conditions. The different curves correspond to the flux of edge and screw densities on different slip systems in the crystal.

to the deduction that the number of edge dislocations in the DD simulation volume cannot have changed significantly. The dislocation configurations within the DD volume do not even have to be considered to come to this conclusion.

According to the continuum model, the edge density begins to accumulate only when the screw density begins to flow. The same behaviour is observed in the DD simulations. The continuum model somewhat underestimates the edge dislocation density level on the primary slip system found in the DD simulations; however, the rates of edge density growth are similar. The continuum model is unable to predict the small increase in the edge dislocation density on the secondary and tertiary slip systems seen towards the end of the DD simulation. In the DD simulations, close encounters between dislocations can lead to large fluctuations in the local stress field causing certain screw segments to move before the far-field stress has reached a level needed to induce a global response from the screw density; a feature not captured by the continuum model.

The screw and edge dislocation flux histories are also well predicted by the continuum model. Not only is the activation of the edge and screw density on the primary slip system captured, but the activation of edge dislocation density on the secondary and tertiary slip systems is also in good agreement with the DD simulations. A feature of the DD simulations that the model is able to capture uniquely is the order of magnitude increase in the edge dislocation flux of the primary slip system towards the end of the simulation. There is only a small increase in the stress as the material reaches the macro-yield point, but the edge dislocation flux increases dramatically due to an order of magnitude increase in the edge

dislocation density, which does not significantly increase the resistance of that same density to glide. Through the explicit use of Orowan's relation in equation (8), this dislocation density based model is able to capture the behaviour correctly. To our knowledge, there is no existing strength-based crystal plasticity model that would be able to reproduce this feature of the edge flux history.

The dislocation density based continuum model is able to reproduce many of the important features of the DD simulation with a great decrease in computational cost. The DD simulations required 50 CPU hours on a Compaq workstation with an ev67 processor, whereas the continuum simulations required less than a CPU minute on a Pentium III based desktop computer. The superior computational efficiency of the continuum model is not without a price. The exact dislocation positions detailed in the DD simulations are lost in the continuum model.

At the low strain levels that were used to determine the material constants, there was not enough sensitivity to all of the material parameters for the plastic behaviour to be extrapolated to large strains. Particularly, there was not enough glide activity among the screw dislocation densities to determine their interaction with the forest density, and the zero coefficients in the $H_{\mathrm{ee}}^{\alpha\beta}$ and $H_{\mathrm{es}}^{\alpha\beta}$ matrices that best fit the screw dislocation density evolution at these strains will most likely not hold at larger strains where loop multiplication may dominate the evolution. However, the ability of the model to reproduce the DD results means that the correct scaling laws for density evolution at these low strain levels are included in the continuum model, and a meaningful method of interpreting DD simulations results within the context of continuum plasticity has been established. By conducting a series of DD simulations reaching larger strain levels, material constants could be obtained and evolution equations evaluated from a single orientation by fitting the slip activity on all the slip systems simultaneously, rather than conducting a large number of simulations in an attempt to isolate specific interaction coefficients. The latent hardening characteristics of the crystal, the evolution of strength on a particular slip system due to slip on another, would surface from the relative activity of the secondary and tertiary slip systems with changing dislocation density and stress states. Accurate DD simulations would only need to reach moderate strains to determine all the material constants of the continuum model required to accurately extrapolate the plastic behaviour of the crystal at large strains. The accuracy of the DD simulations is being continuously improved by appealing to atomistic investigations of dislocation mobility in BCC metals [17, 18].

6. Conclusion

There are currently two paradigms within the multi-scale materials modelling framework. There is an embedding scheme in which fine scale models are embedded within coarse grained models, and both are solved simultaneously. There is also an information passing scheme in which coarse grained models are informed by the simulation results of fine scale models with both models run independently. Following the second paradigm, a dislocation density based continuum model of crystal plasticity is developed to interpret DD simulation results. Evolution equations for the growth of crystallographic density and their average segment lengths are derived from observations in DD simulations, and the material constants are determined by fitting the slip activity and dislocation evolution on all the slip systems simultaneously from simple tension simulations on a single orientation.

The agreement of the fitted continuum model and DD simulations for another orientation demonstrates that the continuum model captures the underlying physics in the DD simulations and that the fitting procedure is robust at these strain levels. Comparisons of the two models

enabled efficient extraction of the critical phenomena and functional dependences concerning the growth of dislocation density during the Stage 0 deformation of BCC metals, characterized by the elongation of screw dislocations, through the motion of edge dislocations and by the multiplication of dislocation sources with ensuing screw motion.

The strength of the current dislocation density based continuum model lies in its ability to differentiate between the behaviour of edge and screw densities providing a consistent framework to model all deformation stages of BCC single crystals; however, more work is needed to extend DD simulations to moderately larger strains and higher dislocation densities before a continuum model informed by information passing from the DD simulations will be able to accurately extrapolate the material behaviour at large strains. This study focused mainly on the growth of dislocation density at strains of the order of 0.1%. Studies must be conducted that also reflect dislocation recovery processes and dislocation forest interactions of screw dislocation densities whose influences were observed to be negligible in the Stage 0 deformation regime.

Acknowledgments

The authors would like to thank Dr R Becker for his comments and suggestions. This work was performed under the auspices of the US Department of Energy by the University of California, Lawrence Livermore National Laboratory under Contract No W-7405-Eng-48.

References

[1] Mathur K K and Dawson P R 1989 On modeling the development of crystallographic texture in bulk forming processes *Int. J. Plasticity* **5** 67–94
[2] Bassani J L and Wu T Y 1991 Latent hardening in single crystals ii. analytical characterization and predictions *Proc. R. Soc.* A **435** 21–41
[3] Bronkhorst C A, Kalidindi S R and Anand L 1992 Polycrystalline plasticity and the evolution of crystallographic texture in FCC metals *Phil. Trans. R. Soc.* A **341** 443–77
[4] Cuitiño A M and Ortiz M 1992 Computational modelling of single crystals *Modelling Simul. Mater. Sci. Eng.* **1** 225–63
[5] Arsenlis A and Parks D P 2002 Modeling the evolution of crystallographic dislocation density in crystal plasticity *J. Mech. Phys. Solids* **50** 1979–2009
[6] Tang M, Kubin L P and Canova G R 1998 Dislocation mobility and the mechanical response of bcc single crystals: a mesoscopic approach *Acta Mater.* **46** 3221–35
[7] Tang M, Devincre B and Kubin L P 1999 Simulation and modeling of forest hardening in body centre cubic crystals at low temperature *Modelling Simul. Mater. Sci. Eng.* **7** 893–908
[8] Kocks U F, Argon A S and Ashby M F Thermodynamics and kinetics of slip *Prog. Mater. Sci.* **19**
[9] Boudet A and Kubin L P 1975 Exhaustion mechanisms in the preyield domain of niobium single crystals at low temperatures *J. Phys.* (France) **36** 823–33
[10] Tang M, Fivel M and Kubin L P 2001 From forest hardening to strain hardening in body centered cubic single crystals: simulation and modeling *Mater. Sci. Eng.* A **309–310** 256–60
[11] Friedel J 1964 *Dislocations* (Oxford: Pergamon)
[12] Tang M and Kubin L P 2001 Boundary conditions for dislocation dynamics simulations and Stage 0 of bcc metals at low temperature *Mater. Res. Soc. Symp. Proc.* AA1.2, p 677
[13] Asaro R J and Rice J R 1977 Strain localization in ductile single crystals *J. Mech. Phys. Solids* **25** 309–38
[14] Püschl W 2000 The flow stress contribution of dislocation 'forest' in bcc lattices *Phil. Mag. Lett.* **80** 199–203
[15] Johnston W G and Gilman J 1959 Dislocation velocities, dislocation densities, and plastic flow in lithium fluoride crystals *J. Appl. Phys.* **30** 129–44
[16] Franciosi P and Zaoui A 1982 Multislip in FCC crystals: a theoretical approach compared with experimental data *Acta Metall.* **30** 1627–37
[17] Duesberry M S and Vitek V 1998 Plastic anisotropy in bcc transition metals *Acta Mater.* **42** 1481–92
[18] Yang L H, Soderlind P and Moriarty J A 2001 Accurate atomistic simulation of $(a/2)\langle 1\,1\,1\rangle$ screw dislocations and other defects in bcc tantalum *Phil. Mag.* A **81** 1355–85